

Dynamic loading criteria in actuator selection for desired dynamic performance

ALAN BOWLING^{1,*} and OUSSAMA KHATIB²

¹ *University of Notre Dame, Notre Dame, IN 46556, USA*

² *Stanford University, Stanford, CA 94305, USA*

Received 3 December 2002; accepted 21 February 2003

Abstract—This article presents two methods for selecting actuators based on the dynamic loading criteria which yield a manipulator with a desired level of dynamic performance. Here, dynamic performance is measured in terms of a robot's acceleration and force capabilities, which describe its ability to accelerate the end-effector and to apply forces to the environment, given the limitations on its actuator torques. The *Dynamic Capability Equations* are used to model the relationship between actuator torque capacities and the acceleration and force capabilities, because they treat linear and angular quantities in a consistent and physically meaningful way. This article discusses actuator selection for a single configuration, as well as for multiple configurations.

Keywords: Actuator selection; dynamic performance; dynamic loading; design; dynamics.

1. INTRODUCTION

The actuators in a robot are key factors in determining its dynamic performance. It is important to choose motors with enough torque capacity to give the mechanism a level of performance sufficient to perform the desired tasks. This article presents two actuator selection methods which produce a manipulator with a desired level of dynamic performance.

Many different criteria are involved in the selection of actuators, such as power requirements, reliability, weight and cost. This article explores the dynamic loading/performance criteria, which is especially important in the design of high-performance manipulators [1]. Here, dynamic performance is measured in terms of a robot's acceleration and force capabilities. They describe a manipulator's ability to accelerate its end-effector and to apply forces to the environment at the end-effector.

*To whom correspondence should be addressed. E-mail: abowling@nd.edu

These capabilities determine a mechanism's capacity for manipulating grasped and non-grasped objects.

The model which relates acceleration and force capabilities to the actuator torque capacities is referred to as the *Dynamic Capability Equations*. A key feature in the development of these equations is the treatment of linear and angular quantities in a manner which resolves the inhomogeneities or differences in units between linear and angular motions.

The challenge in actuator selection is caused by the difficulty in isolating the actuator torque capacities in the model, which can be expressed as:

$$\mathbf{f}(\Upsilon_{\text{bound}}, \dots) = \mathbf{0}, \quad (1)$$

where the vector \mathbf{f} is a function of the vector containing the bounds on the actuator torque capacities, Υ_{bound} , as well as other manipulator parameters. Isolating Υ_{bound} would yield:

$$\mathbf{f}(\dots) = \Upsilon_{\text{bound}}, \quad (2)$$

easily solvable for the correct actuators. However, a solution such as (2) has not been found. This article presents two iterative solutions.

In the following sections an overview of the Dynamic Capability Equations and hypersurface is given first. The actuator selection methods are then developed for a single configuration and then for multiple configurations of a manipulator. Examples of the single and multiple configuration cases are presented next. Only non-redundant manipulators are considered here.

2. DYNAMIC PERFORMANCE

In this section the relationship between dynamic performance and actuator torque capacity is discussed. There have been many important studies of this relationship, resulting in a number of different characterizations, including: the *dynamic manipulability ellipsoid* [2], the *acceleration hyperparallelepiped* [3], the *acceleration radius* [4], the *Dynamic Load Carrying Capacity (DLCC)* [5] and *Acceleration Set Theory* [6].

In the studies mentioned above, except for the DLCC, a geometric representation of the actuator torque bounds is mapped into accelerations using relations from the dynamic model. Figure 1 shows examples of two of these studies, the dynamic manipulability ellipsoid and the acceleration parallelepiped, for a 2-d.o.f. manipulator. The acceleration parallelepiped [3] is the image in acceleration space of the rectangular torque bounds. It represents all possible achievable end-effector accelerations. The rectangle and parallelepiped are not centered at the origin and operational point because of the effect of gravity. The dynamic manipulability ellipsoid is the image in acceleration space of the dashed circle inscribed within the torque bounds.

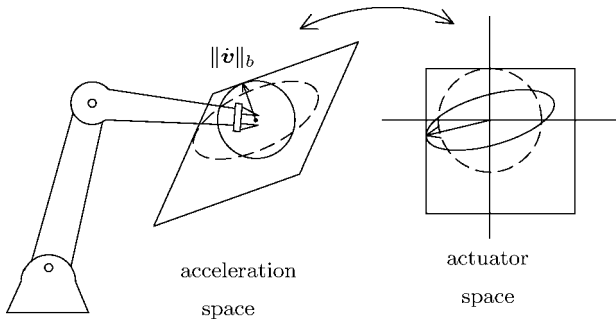


Figure 1. 2-d.o.f. accelerations.

In Fig. 1, the circle inscribed within the acceleration parallelepiped represents an isotropic or balanced acceleration capability. Its image in actuator space is an ellipsoid. The radius of the circle, referred to as the isotropic or *balanced acceleration*, $\|\dot{v}\|_b$, is limited by the smallest actual achievable acceleration. *The balanced acceleration gives the magnitude of acceleration which is guaranteed to be achievable in every direction.* The contact point between the circle and parallelepiped defines the *limiting* or *worst-case direction* of motion, indicated by the vectors shown in Fig. 1. The side of the parallelepiped in contact gives the *limiting actuator*, the motor which saturated attempting to produce the balanced acceleration in the worst-case direction.

The analyses discussed up to this point cannot be directly applied to the 3-d.o.f. manipulator shown in Fig. 2. This is because its end-effector motions are described in terms of linear and angular quantities. Mixing these quantities into one representation of acceleration, a sphere for instance, yields a radius or balanced acceleration with mixed units, which has no physical meaning. It is unclear how to interpret the dynamic manipulability ellipsoid for the 3-d.o.f. mechanism. Acceleration Set Theory [6] does not address the inhomogeneity problem. The acceleration hyperparallelepiped mixes linear and angular accelerations along its edges and faces, making it difficult understand. The issues surrounding the unitary inhomogeneity problem have been the subject of a large body of work including [7–10].

The DLCC study [5] is unaffected by the inhomogeneity problem; however, it only considers the performance required to move in one direction along a particular path. Here, a description of the performance in every direction is preferred.

In order to address the inhomogeneity problem, linear and angular quantities are kept separate in the development of the Dynamic Capability Equations. A consequence of this approach is that acceleration capability cannot be measured by a single number, the radius of a circle or sphere. The proposed analysis produces a curve which describes the relationship between balanced linear and angular accelerations.

In addition, the Dynamic Capability Equations also describe for capability, as well as the effect of end-effector velocities on the acceleration and force capabilities. The

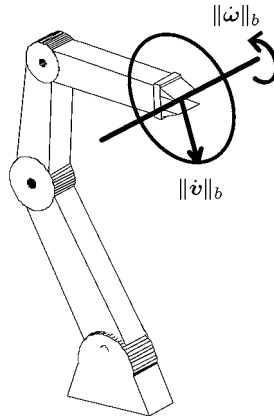


Figure 2. 3-d.o.f. accelerations.

velocity effects include the *speed–torque* curve, which describes the reduction of torque capacity due to rotor velocity, and the Coriolis and centrifugal forces.

The Dynamic Capability Equations are:

$$\mathbb{A} \begin{bmatrix} \|\dot{\mathbf{v}}\| \\ \|\dot{\boldsymbol{\omega}}\| \end{bmatrix} + \mathbb{C} (\|\mathbf{v}\|^2, \|\boldsymbol{\omega}\|^2) + \mathbb{F} \begin{bmatrix} \|\mathcal{F}\| \\ \|\mathcal{M}\| \end{bmatrix} \leq \mathbb{T}, \tag{3}$$

where

$$\mathbb{T} = \begin{bmatrix} \boldsymbol{\Upsilon}_{\text{bound}} \\ \boldsymbol{\Upsilon}_{\text{bound}} \end{bmatrix} - \mathbb{G}. \tag{4}$$

\mathbb{A} and \mathbb{F} are $2n \times 2$ matrices, for an n -d.o.f. manipulator, obtained from the inertial properties and the manipulator Jacobian. \mathbb{C} is a vector derived from the Coriolis/centrifugal terms and the speed–torque curves, and \mathbb{G} contains the gravity forces. The manipulator is assumed to have n actuators, thus $\boldsymbol{\Upsilon}_{\text{bound}}$ has dimension n . \mathbf{v} and $\boldsymbol{\omega}$ are the linear and angular end-effector velocity vectors, and $\dot{\mathbf{v}}$ and $\dot{\boldsymbol{\omega}}$ are the corresponding accelerations. The vectors \mathcal{F} and \mathcal{M} represent the contact forces and moments at the end-effector. Equation (3) is considered row by row or element by element. The Dynamic Capability Equations are discussed in the Appendix and in [11–13].

A section of the *Dynamic Capability Hypersurface* defined by (3), obtained using $\|\boldsymbol{\omega}\| = \|\mathcal{F}\| = \|\mathcal{M}\| = \mathbf{0}$, is shown in Fig. 3. The surface was obtained using the model for the PUMA 560 given in [14]. The worst-case directions of motion are shown as the line segments emanating from the end-effector of PUMA 560 in Fig. 4. The limiting actuator is indicated by the numeric label, 2, on the surface of Fig. 3.

The curve in the $\|\dot{\mathbf{v}}\|_b$ - $\|\dot{\boldsymbol{\omega}}\|_b$ plane of Fig. 4, gives the combinations of the magnitudes of linear and angular acceleration achievable in every direction, at zero velocity, which saturate the second actuator. The limiting case is to accelerate in the worst-case directions, labeled $\dot{\mathbf{v}}$ and $\dot{\boldsymbol{\omega}}$ in Fig. 4, with the magnitudes indicated by the curve.

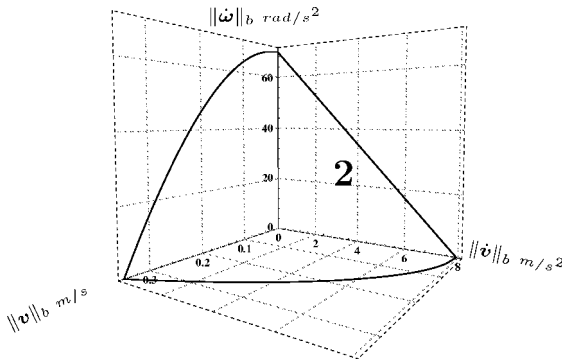


Figure 3. PUMA 560 dynamic capability surface.

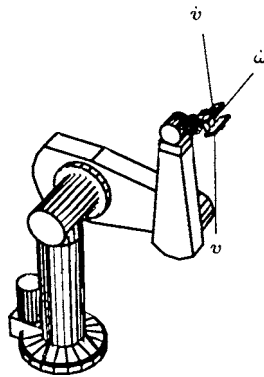


Figure 4. Worst-case motion directions.

Table 1. Statistical surface configurations

Joint	Angle set
1	{0}
2	{45°, 0°, -45°, -90°, -135°, -180°}
3	{-45°, 0°, 45°, 90°, 135°}
4	{0°, 90°, 180°, 270°}
5	{90°, 45°, -45°, -90°}
6	{0}

The remainder of the surface describes the bounds on acceleration capability when accelerating from a particular linear velocity. The shape of the surface indicates that acceleration capability decreases to zero as linear velocity increases. The limiting case is when the velocity is in the v direction shown in Fig. 4.

The workspace of a manipulator can be characterized by statistically analyzing the Dynamic Capability Hypersurface at several different configurations. The statistical hypersurfaces are generated using the distance to each surface along lines

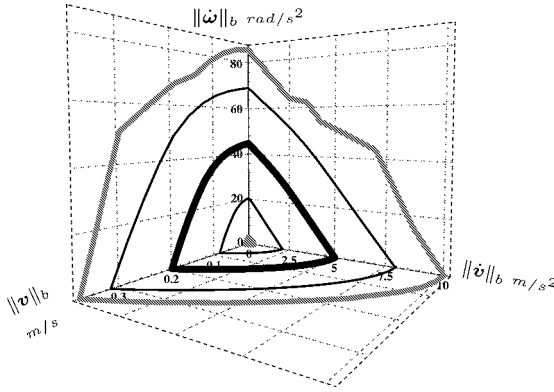


Figure 5. PUMA 560 statistical surface.

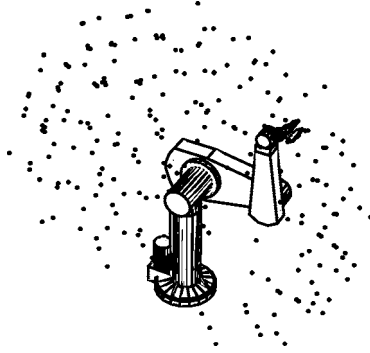


Figure 6. Statistical surface configurations.

extending radially out from the origin. Sections of the statistical hypersurfaces, where $\|\omega\| = \|\mathcal{F}\| = \|\mathcal{M}\| = \mathbf{0}$, are shown in Fig. 5 for 480 configurations in the workspace of the PUMA 560 manipulator. The dots in Fig. 6 show the operational point for these configurations, which are generated from permutations of the joint angles shown in Table 1.

The innermost and outermost curves in Fig. 5 show the outlines of the minimum and maximum surfaces. The minimum surface is small because some of the configurations in the set are close to kinematic singularities. The curves nearest the maximum and minimum represent the deviation surfaces, and the remaining curves show the average surface.

3. ACTUATOR SELECTION

A number of actuator selection methods have addressed dynamic performance. Many of these are based on the characterizations discussed in Section 2. These include [15], which is nearest to the proposed method, but it does not address the inhomogeneity problem. A path-based optimization driven by the DLCC is

presented in [16]. A method based on Acceleration Set Theory is discussed in [17]; however, it is only applicable to 2-d.o.f. manipulators. Shiller and Sundar [18] use optimization and the Acceleration Parallelepiped to find actuators which decrease the time taken to traverse a particular path.

The idea behind the development of the Dynamic Capability Equations and hypersurface was to describe manipulator performance given a set of actuators; given $\mathbf{Y}_{\text{bound}}$ find $\|\dot{\mathbf{v}}\|$, $\|\dot{\boldsymbol{\omega}}\|$, $\|\mathcal{F}\|$, $\|\mathcal{M}\|$, $\|\mathbf{v}\|$ and $\|\boldsymbol{\omega}\|$. In this section, the goal is to choose the actuators given a desired level of performance. The desired performance is specified by *performance points*:

$$p_i = (\|\dot{\mathbf{v}}\|_i, \|\dot{\boldsymbol{\omega}}\|_i, \|\mathcal{F}\|_i, \|\mathcal{M}\|_i, \|\mathbf{v}\|_i, \|\boldsymbol{\omega}\|_i), \quad (5)$$

p_i represents a desired point on the Dynamic Capability Hypersurface. Several performance points are used to describe the desired shape of the hypersurface. The proposed actuator selection methods insure that all points lie on or beneath the hypersurface. However, the proposed procedures cannot currently satisfy a performance point where neither $\|\mathbf{v}\|$ or $\|\boldsymbol{\omega}\|$ is equal to zero.

Substituting a performance point into the Dynamic Capability Equations yields:

$$\mathbb{A} \begin{bmatrix} \|\dot{\mathbf{v}}\|_i \\ \|\dot{\boldsymbol{\omega}}\|_i \end{bmatrix} + \mathbb{C} (\|\mathbf{v}\|_i^2, \|\boldsymbol{\omega}\|_i^2) + \mathbb{F} \begin{bmatrix} \|\mathcal{F}\|_i \\ \|\mathcal{M}\|_i \end{bmatrix} + \mathbb{G} \leq \begin{bmatrix} \mathbf{Y}_{\text{bound}} \\ \mathbf{Y}_{\text{bound}} \end{bmatrix}. \quad (6)$$

Also note that

$$\mathbb{A} = \mathbb{A}(\mathbf{m}_{\text{motor}}(\mathbf{Y}_{\text{bound}}), \mathbf{I}_{\text{motor}}(\mathbf{Y}_{\text{bound}}), \dots), \quad (7)$$

$$\mathbb{C} = \mathbb{C}(\mathbf{m}_{\text{motor}}(\mathbf{Y}_{\text{bound}}), \mathbf{I}_{\text{motor}}(\mathbf{Y}_{\text{bound}}), \dots), \quad (8)$$

$$\mathbb{G} = \mathbb{G}(\mathbf{m}_{\text{motor}}(\mathbf{Y}_{\text{bound}}), \mathbf{I}_{\text{motor}}(\mathbf{Y}_{\text{bound}}), \dots), \quad (9)$$

where $\mathbf{m}_{\text{motor}}$ and $\mathbf{I}_{\text{motor}}$ contain the mass and inertias of the actuators' rotors and stators. Given a particular configuration and set of actuators, (6) can be evaluated to determine whether the actuators satisfy the performance point.

It is difficult to isolate $\mathbf{Y}_{\text{bound}}$ in (6) because \mathbb{A} and \mathbb{C} are highly nonlinear functions see Appendix. This complicates actuator selection, making it necessary to use an iterative solution, two of which are discussed in the next sections.

3.1. Actuator selection heuristic

The advantage of the heuristic is that it selects actuators from a discrete list. Thus it can find a set of real actuators, from real actuator data, which satisfy the performance requirements. Any actuators can be included in the list; however, the performance of the procedure is dependent upon the entries.

A flow chart of the heuristic is shown in Fig. 7. First, the mass properties of the actuators are set to zero. The initial actuators are chosen as the smallest ones which can compensate for gravitational forces. Equation (6) is then evaluated for each performance point. If all points are satisfied, the procedure stops. If not, the limiting actuator for the least satisfied performance point is changed to the closest

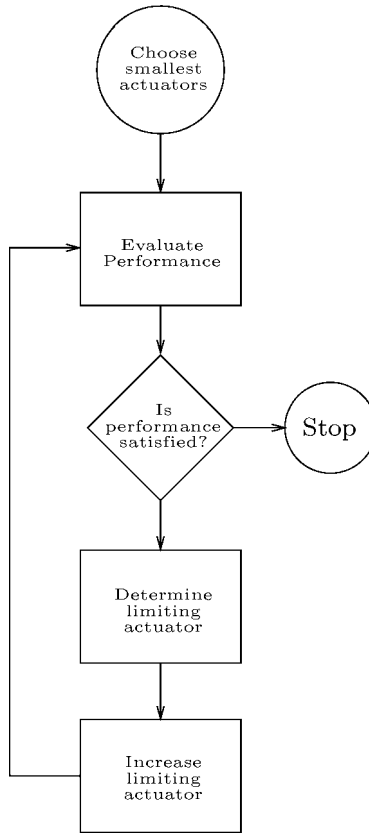


Figure 7. Actuator selection heuristic.

actuator with a higher torque capacity. Equation (6) is reevaluated and the process begins again.

There are many variations on this heuristic which may yield different solutions than the proposed method. The important aspect of the procedure is that at each iteration changes are made based on the limiting actuator information.

3.2. Actuator optimization procedure

The optimization procedure finds actuators which yield a Dynamic Capability Hypersurface that fits the performance points as closely as possible. This method requires the definitions for $\mathbf{m}_{\text{motor}}(\mathbf{Y}_{\text{bound}})$, $\mathbf{I}_{\text{motor}}(\mathbf{Y}_{\text{bound}})$ and any other actuator-dependent quantities in (6).

This method also requires a means for determining the extent to which a performance point is satisfied. This is accomplished by assigning a magnitude, the scalar α_i , to each performance point:

$$\alpha_i p_i = \alpha_i (\|\dot{\mathbf{v}}\|_i, \|\dot{\boldsymbol{\omega}}\|_i, \|\mathcal{F}\|_i, \|\mathcal{M}\|_i, \|\mathbf{v}\|_i, \|\boldsymbol{\omega}\|_i). \quad (10)$$

Substituting (10) into the Dynamic Capability Equations yields

$$\alpha_i \mathbb{A} \begin{bmatrix} \|\dot{\mathbf{v}}\|_i \\ \|\dot{\boldsymbol{\omega}}\|_i \end{bmatrix} + \alpha_i^2 \mathbb{C} (\|\mathbf{v}\|_i^2, \|\boldsymbol{\omega}\|_i^2) + \alpha_i \mathbb{F} \begin{bmatrix} \|\mathcal{F}\|_i \\ \|\mathcal{M}\|_i \end{bmatrix} + \mathbb{G} \leq \begin{bmatrix} \boldsymbol{\Upsilon}_{\text{bound}} \\ \boldsymbol{\Upsilon}_{\text{bound}} \end{bmatrix}. \quad (11)$$

The relations in (11) are quadratic with respect to α_i . The performance point is satisfied when the smallest positive root for α_i obtained from (11) satisfies:

$$\alpha_i \geq 1. \quad (12)$$

The scalar α_i can also be used in the heuristic procedure, where the least satisfied performance point yields the smallest value for α_i .

The limits on the range of the torque capacity of each actuator are expressed as:

$$\boldsymbol{\Upsilon}_{\text{min}} \leq \boldsymbol{\Upsilon}_{\text{bound}} \leq \boldsymbol{\Upsilon}_{\text{max}}, \quad (13)$$

considered element by element. One possibility for defining $\boldsymbol{\Upsilon}_{\text{min}}$ is to use the actuators chosen during the start of the heuristic procedure.

The cost function for this optimization should minimize the size of each actuator:

$$\text{cost} = \frac{\boldsymbol{\Upsilon}_{\text{bound}_1}}{\boldsymbol{\Upsilon}_{\text{min}_1}} + \dots + \frac{\boldsymbol{\Upsilon}_{\text{bound}_n}}{\boldsymbol{\Upsilon}_{\text{min}_n}}. \quad (14)$$

The square of each term can also be summed; however, this will result in a larger weighting for the larger terms in the cost function. If all of the actuator torques have the same units, then the normalization in (14) can be omitted.

In summary, the decision variables for the optimization are $\{\boldsymbol{\Upsilon}_{\text{bound}_1}, \dots, \boldsymbol{\Upsilon}_{\text{bound}_n}, \alpha_1, \dots, \alpha_k\}$ where k is the number of performance points. The cost function is given in (14), and the constraints on the optimization are given in (13), (12) and (11). One set of the relations in (11) and (12) is needed for each performance point. Note that this procedure is only guaranteed to find locally optimal solutions.

3.3. Single configuration example

In this example actuators are chosen to improve the performance of the PUMA 560 manipulator shown in Fig. 4, which is reproduced in Fig. 8 by the surface labeled ‘a’. The desired level of performance is specified by the following performance points:

$$p_1 = (9.8 \text{ m/s}^2, 0, 0, 0, 0, 0), \quad (15)$$

$$p_2 = (0, 75 \text{ rad/s}^2, 0, 0, 0, 0), \quad (16)$$

$$p_3 = (0, 0, 1 \text{ m/s}, 0, 0, 0), \quad (17)$$

indicated by the symbol ‘ \odot ’ in Fig. 8.

The heuristic chose actuators from the list given in Table 2. The actuators for the PUMA 560 were included in the heuristic actuator selection. Also note that the PUMA 560 model used here [14] only allowed for changes in the peak torque, rotor inertia and the max rotor angular velocity.

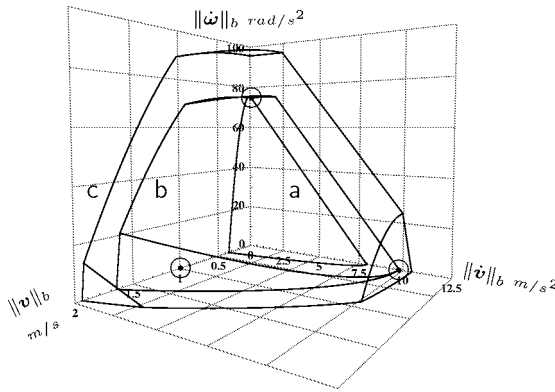


Figure 8. Actuator selection for PUMA 560.

Table 2.

List of possible actuators

New			PUMA 560 original		
Peak torque (N m)	Max speed (rad/s)	Rotor inertia (kgm ²)	Peak torque (N m)	Max speed (rad/s)	Rotor inertia (kgm ²)
0.0004	2000	1.1e-8			
0.004	1780	2.7e-8			
0.01	1371	4.8e-8			
0.1	548	9.4e-7			
0.2	1885	1.6e-7	0.26	302	3.3e-5
0.4	1414	2.7e-7	0.30	302	3.5e-5
0.6	1204	3.6e-7			
0.8	1079	1.4e-6	1.46	90	2.9e-4
1.2	922	2.0e-6	1.62	114	2.9e-4
1.6	859	2.5e-6	1.69	100	4.1e-4

The optimization used linear interpolation between the actuators in Table 2 to define the continuous actuator properties, $\mathbf{m}_{\text{motor}}(\Upsilon_{\text{bound}})$ and $\mathbf{I}_{\text{motor}}(\Upsilon_{\text{bound}})$ in (7), (8) and (9). The PUMA 560 motors were omitted from the optimization actuator list in order to obtain actuator properties which change monotonically with peak torque. A non-monotonic list causes problems for the optimization routine when linear interpolation is used.

Figure 8 shows that the heuristic and optimization procedures can select actuators which satisfy the desired performance. Labels ‘b’ and ‘c’ in Fig. 8 indicate the surfaces obtained using the optimization and heuristic actuator selection methods. The result of the optimization fits the performance points closer than that of the heuristic. Note that the surfaces ‘b’ and ‘c’ are comprised of several ‘patches’; there is at least one limiting actuator for each surface patch.

Also notice that, excluding the PUMA 560 actuators, a comparison of the motors chosen by the heuristic and optimization (Table 3), and the set of possible actuators

Table 3.

Actuator selection results

Joint	Peak torque (N m)		
	Original	Heuristic	Optimization
1	1.46	1.6	1.3
2	1.69	1.2	1
3	1.62	0.4	0.4
4	0.30	0.1	0.04
5	0.26	0.1	0.08
6	0.26	0.004	0.003

(Table 2), shows that the heuristic found the best actuators it could. For instance, for the first joint, the heuristic chose a 1.6 N m actuator, which is as close as is possible to the 1.3 N m actuator found by the optimization. This is also true for the other actuators chosen by the heuristic. In this way the optimization can be used to check the results of the heuristic procedure.

Another interesting result is that all except one of the new actuators chosen by both procedures have a lower peak torque than the original actuators. However, the large differences between the properties of the new and original actuators make it difficult to discern whether the results are solely due to poor selection of actuator torque capacity.

3.4. Workspace considerations

Actuator selection can be carried out on performance points that are referenced to the statistical hypersurfaces. Much of the methods discussed in Sections 3.1 and 3.2 remain the same, except for the constraint in (12). For instance, when considering the average statistical hypersurface, (12) becomes:

$$\sum_j w_j \alpha_{ij} / \sum_j w_j \geq 1, \quad (18)$$

where the subscripts i and j indicate the performance point and the configuration. w_j represents the weighting for the j th configuration, which is $w_j = 1$ for a standard average. Similar expressions can be developed for the other statistical hypersurfaces.

In the heuristic procedure, (18) is used to determine whether a performance point is statistically satisfied. The decision variables for the optimization are $\{\mathbf{Y}_{\text{bound}_1}, \dots, \mathbf{Y}_{\text{bound}_n}, \alpha_{11}, \dots, \alpha_{kp}\}$, where k and p are the number of performance points and configurations. The cost function is given in (14), and the constraints are (18), (13) and (11); one (18) for each performance point and one set of the relations in (11) for each configuration–performance point pair.

Figures 9 and 10 show the results of the statistical actuator selection using the heuristic and optimization procedures for the configurations shown in Fig. 6, and

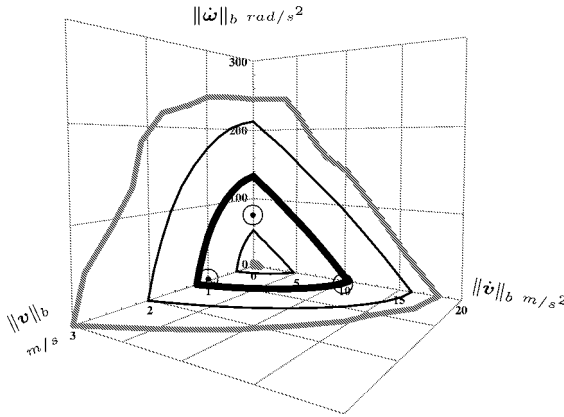


Figure 9. Statistical actuator selection: heuristic.

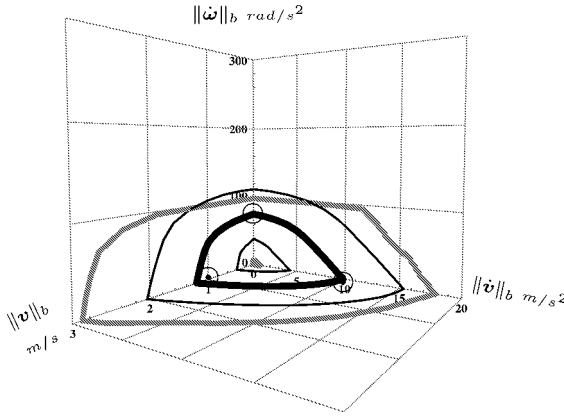


Figure 10. Statistical actuator selection: optimal.

the performance points given in (15), (16) and (17). These points are indicated by the ‘ \odot ’ in Figs 9 and 10. The actuator list given in Table 2, excluding the PUMA 560 actuators, was used for the selection. Both Figs 9 and 10 show that the average statistical hypersurface satisfies the performance points. However, the optimization procedure yielded an average surface closer to the performance points than the heuristic.

4. CONCLUSIONS

This article presented a heuristic and an optimization procedure for selecting actuators which provide a desired level of manipulator dynamic performance. Dynamic performance was measured in terms of a manipulator’s acceleration and force capabilities. The Dynamic Capability Equations were used as the model for actuator selection. The key feature in the development of these equations is that they

treat linear and angular quantities in a consistent and physically meaningful manner. The selection algorithms were developed for single and multiple configurations of the manipulator.

Acknowledgements

Many thanks to Professor Walter Murray (Department of Engineering–Economic Systems, Stanford University) for his assistance with the optimization aspects of this work. Also thanks to Mr Wei Wang (graduate student, Department of Aerospace and Mechanical Engineering, University of Notre Dame) for his help in the preparation of this paper. This work was completed at Stanford University.

REFERENCES

1. J. Vaidya, Motor selection for actuation systems, in: *Proc. 22nd IEEE Combined Electrical/Electronic Insulation Conf. and Electrical Manufacturing and Coil Winding Conf. and Exhibition*, Rosemont, IL, pp. 385–391 (1995).
2. T. Yoshikawa, Dynamic manipulability of robot manipulators, in: *Proc. IEEE Int. Conf. on Robotics and Automation*, St Louis, MO, pp. 1033–1038 (1985).
3. O. Khatib and J. Burdick, Optimization of dynamics in manipulator design: the operational space formulation, *Int. J. Robotics Automat.* **2** (2), 90–98 (1987).
4. T. J. Graettinger and B. H. Krogh, The acceleration radius: a global performance measure for robotic manipulators, *IEEE J. Robotics Automat.* **4** (1), 60–69 (1988).
5. L. T. Wang and B. Ravani, Dynamic load carrying capacity of mechanical manipulators-part i: problem formulation, *J. Dyn. Syst. Meas. Control* **110**, 46–52 (1988).
6. Y. Kim and S. Desa, The definition, determination, and characterization of acceleration sets for spatial manipulators, *Int. J. Robotics Res.* **12** (6), 572–587 (1993).
7. H. Lipkin and J. Duffy, Hybrid twist and wrench control for a robotic manipulator, *J. Mech. Transmissions Automat. Des.* **110**, 138–144 (1988).
8. J. Duffy, Editorial: the fallacy of modern hybrid control theory that is based on ‘orthogonal complements’ of twist and wrench spaces. *J. Robotic Syst.* **7** (2), 139–144 (1990).
9. K. L. Doty, C. Melchiorri, E. M. Schwartz and C. Bonivento, Robot manipulability, *IEEE Trans. Robotics Automat.* **11** (3), 462–468 (1995).
10. K. Kazerounian and J. Rastegar, Object norms: a class of coordinate and metric independent norms for displacements, *Flexible Mech. Dyn. Anal.* **47**, 271–275 (1992).
11. A. Bowling and O. Khatib, The Dynamic Capability Hypersurface: A new tool for analyzing manipulator dynamic performance, *IEEE Trans. Robotics Automat.* (2003) (submitted).
12. A. Bowling and O. Khatib, The motion isotropy hypersurface: a characterization of acceleration capability, in: *Proc. IEEE/RSJ Int. Conf. on Intelligent Robots and Systems*, Victoria, BC, Vol. 2, pp. 965–971 (1998).
13. A. Bowling and O. Khatib, Robot acceleration capability: the actuation efficiency measure, in: *Proc. IEEE Conf. on Robotics and Automation*, San Francisco, CA, Vol. 4, pp. 3970–3975 (2000).
14. B. Armstrong, O. Khatib and J. Burdick, The explicit model and inertial parameters of the puma 560 arm, in: *Proc. IEEE Int. Conf. on Robotics and Automation*, Vol. 1, pp. 510–518 (1986).
15. M. Thomas, H. C. Yuan-Chou and D. Tesar, Optimal actuator sizing for robotic manipulators based on local dynamic criteria, *J. Mech. Transmissions Automat. Des.* **107** (2), 163–169 (1985).

16. R. Kashani and B. Ravani, Optimal sizing of robot actuators based on dynamic load carrying capacity, in: *Proc. 21st Biennial ASME Mechanisms Conf.*, Chicago, IL, Vol. 2, pp. 193–197 (1990).
17. S. Desa and Y.-Y. Kim, Application of acceleration set theory to manipulator design, in: *Proc. 21st Biennial ASME Mechanisms Conf.*, Chicago, IL, pp. 221–228 (1990).
18. Z. Shiller and S. Sundar, Design of robotic manipulators for optimal dynamic performance, in: *Proc. IEEE Int. Conf. on Robotics and Automation*, Sacramento, CA, pp. 344–349 (1991).
19. O. Khatib, Inertial properties in robotic manipulation: an object-level framework, *Int. J. Robotics Res.* **13** (1), 19–36 (1995).

APPENDIX: DYNAMIC CAPABILITY EQUATIONS

This appendix summarizes the results from the development of the Dynamic Capability Equations. More in depth discussions are given in Refs [11, 12]. The development begins with the operational space equations of motion [14]:

$$\Lambda \dot{\boldsymbol{\vartheta}} + \boldsymbol{\mu} + \mathbf{p} + \mathbf{F}_c = \mathbf{F} \quad (\text{A.1})$$

where:

$$\boldsymbol{\vartheta} \triangleq \begin{bmatrix} \mathbf{v} \\ \boldsymbol{\omega} \end{bmatrix} = J \dot{\mathbf{q}}, \quad (\text{A.2})$$

and:

$$\mathbf{F}_c = \begin{bmatrix} \mathcal{F} \\ \mathcal{M} \end{bmatrix}, \quad (\text{A.3})$$

and Λ is the pseudo-kinetic energy matrix representing inertial properties. $\boldsymbol{\mu}$ and \mathbf{p} are the vectors of Coriolis, centrifugal and gravity forces. \mathbf{F} and \mathbf{F}_c are vectors of end-effector forces and moments generated by the actuators and by contact with the environment. J is the manipulator Jacobian and $\dot{\mathbf{q}}$ is the vector of generalized/joint speeds. Note that $\boldsymbol{\vartheta}$ contains an independent set of coordinates. An end-effector load is included in the dynamic model.

The bounds on the actuator torque capacities are expressed as:

$$-\boldsymbol{\Upsilon}_{\text{bound}} \leq \boldsymbol{\Upsilon} \leq \boldsymbol{\Upsilon}_{\text{bound}}, \quad (\text{A.4})$$

where $\boldsymbol{\Upsilon}$ is the vector of actuator torques and each element in $\boldsymbol{\Upsilon}_{\text{bound}}$ is a constant. The relationship between joint and end-effector forces is:

$$\boldsymbol{\Gamma} = J^T \mathbf{F}, \quad (\text{A.5})$$

and the relationship between joint and actuator torques is:

$$\boldsymbol{\Gamma} = \mathbf{G}^T \boldsymbol{\Upsilon}, \quad (\text{A.6})$$

where \mathbf{G} is a matrix describing the transmission system and is assumed to be invertible. Equations (A.5) and (A.6) give the *actuator Jacobian*, J_a , defined as:

$$J_a = J \mathbf{G}^{-1}, \quad \text{where} \quad \boldsymbol{\Upsilon} = J_a^T \mathbf{F}. \quad (\text{A.7})$$

Combining equations (A.1), (A.4) and (A.7) yields the desired *constraint equations*:

$$\mathbf{\Upsilon}_{\text{lower}} \leq E_v \dot{\mathbf{v}} + E_w \dot{\boldsymbol{\omega}} + \mathcal{E}_{\mathcal{F}} \mathcal{F} + \mathcal{E}_{\mathcal{M}} \mathcal{M} + \mathbf{h} \leq \mathbf{\Upsilon}_{\text{upper}}, \quad (\text{A.8})$$

where:

$$E = [E_v \ E_w] = J_a^T \Lambda, \quad (\text{A.9})$$

$$\mathcal{E} = [\mathcal{E}_{\mathcal{F}} \ \mathcal{E}_{\mathcal{M}}] = J_a^T, \quad (\text{A.10})$$

and:

$$\mathbf{h} = J_a^T \boldsymbol{\mu}, \quad (\text{A.11})$$

$$\mathbf{\Upsilon}_{\text{upper}} = \mathbf{\Upsilon}_{\text{bound}} - J_a^T \mathbf{p}, \quad (\text{A.12})$$

$$\mathbf{\Upsilon}_{\text{lower}} = -\mathbf{\Upsilon}_{\text{bound}} - J_a^T \mathbf{p}. \quad (\text{A.13})$$

Inclusion of the speed-torque curve velocity information is discussed in detail in Refs [11, 12].

The analysis of balanced motions and forces using (A.8), yields simple formulas for the elements of \mathbb{A} and \mathbb{F} in (3):

$$\begin{aligned} \mathbb{A}_{i,1} \\ \text{and} \\ \mathbb{A}_{i+n,1} \end{aligned} = \sqrt{\sum_{j=1}^r E_{ij}^2} \quad \begin{aligned} \mathbb{A}_{i,2} \\ \text{and} \\ \mathbb{A}_{i+n,2} \end{aligned} = \sqrt{\sum_{j=r+1}^n E_{ij}^2}, \quad (\text{A.14})$$

and

$$\begin{aligned} \mathbb{F}_{i,1} \\ \text{and} \\ \mathbb{F}_{i+n,1} \end{aligned} = \sqrt{\sum_{j=1}^r \mathcal{E}_{ij}^2} \quad \begin{aligned} \mathbb{F}_{i,2} \\ \text{and} \\ \mathbb{F}_{i+n,2} \end{aligned} = \sqrt{\sum_{j=r+1}^n \mathcal{E}_{ij}^2}, \quad (\text{A.15})$$

where $i = (1, \dots, n)$, \mathbf{v} and \mathcal{F} have dimension r . \mathbb{G} in (4) is defined as:

$$\mathbb{G} = \begin{bmatrix} J_a^T \mathbf{p} \\ -J_a^T \mathbf{p} \end{bmatrix}. \quad (\text{A.16})$$

Analysis of the velocity effects depends on the performance point. The vector of velocity dependent terms can be expressed as:

$$\mathbf{h} = \begin{bmatrix} \left[\begin{array}{c} \mathbf{v}^T \\ \boldsymbol{\omega}^T \end{array} \right]^T H_1 \left[\begin{array}{c} \mathbf{v} \\ \boldsymbol{\omega} \end{array} \right] \\ \vdots \\ \left[\begin{array}{c} \mathbf{v}^T \\ \boldsymbol{\omega}^T \end{array} \right]^T H_n \left[\begin{array}{c} \mathbf{v} \\ \boldsymbol{\omega} \end{array} \right] \end{bmatrix}, \quad (\text{A.17})$$

where:

$$H_j = \begin{bmatrix} H_{jv} & H_{jv\boldsymbol{\omega}} \\ H_{jv\boldsymbol{\omega}}^T & H_{j\boldsymbol{\omega}} \end{bmatrix}. \quad (\text{A.18})$$

If $\|\boldsymbol{\omega}\| = 0$, then:

$$\mathbb{C}_j = \lambda_{j \max \mathbf{v}} \|\mathbf{v}\|_i^2, \quad (\text{A.19})$$

$$\mathbb{C}_{j+n} = -\lambda_{j \min \mathbf{v}} \|\mathbf{v}\|_i^2, \quad (\text{A.20})$$

where $\lambda_{j \max \mathbf{v}}$ and $\lambda_{j \min \mathbf{v}}$ are the maximum and minimum eigenvalues of $H_{j\mathbf{v}}$.

If $\|\mathbf{v}\| = 0$, then:

$$\mathbb{C}_j = \lambda_{j \max \boldsymbol{\omega}} \|\boldsymbol{\omega}\|_i^2, \quad (\text{A.21})$$

$$\mathbb{C}_{j+n} = -\lambda_{j \min \boldsymbol{\omega}} \|\boldsymbol{\omega}\|_i^2, \quad (\text{A.22})$$

where $\lambda_{j \max \boldsymbol{\omega}}$ and $\lambda_{j \min \boldsymbol{\omega}}$ are the maximum and minimum eigenvalues of $H_{j\boldsymbol{\omega}}$.

Further details of the velocity solution are given in [11, 12].

ABOUT THE AUTHORS



Alan Bowling received a BS degree in Aerospace Engineering from the University of Texas at Austin in 1988, and MS and PhD degrees from Stanford University in 1992 and 1998, respectively. He pursued entrepreneurial activities from 1998 through 2001. In 2001 he joined the Department of Aerospace and Mechanical Engineering at the University of Notre Dame. His research interests include robotics, performance analysis and systems engineering.



Oussama Khatib received his PhD in 1980 from Sup 'Aero, Toulouse, France. He is a Professor of Computer Science at Stanford University. His research is in human-centered robotics, human-friendly robot design, dynamic simulations and haptic interactions. His exploration in this research ranges from the autonomous ability of a robot to cooperate with a human to the haptic interaction of a user with an animated character or a surgical instrument. Professor Khatib was the Program Chair of ICRA2000 (San Francisco) and Co-Editor of 'The Robotics Review'. He is the President of the International Foundation of Robotics Research, IFRR and Co-Editor of STAR, Springer Tracts in Advanced Robotics. Professor Khatib is a 'Distinguished Lecturer' of IEEE and a recipient of the JARA Award.